Massachusetts Department of Transportation (MassDOT)
and
University of Connecticut

Evaluation & Mitigation Methods for the Prevention of Cement Concrete Deterioration due to Pyrrhotite
Part 1

Final Report

Principal Investigator
Kay Wille
Professor and Interim Director, School of CEE, UConn
261 Glenbrook Rd, Storrs, CT 06269
860-486-3594
kay.wille@uconn.edu

Project Champion/Technical Representative
Jason Robertson
Director of Research and Materials, MassDOT
(857) 368-3467
jason.robertson@dot.state.ma.us

Richard Mulcahy
Materials Evaluation and Research Engineer
MassDOT Research and Materials Laboratory
(857) 368-3422
richard.mulcahy@dot.state.ma.us

Administrative Contact
Mass Venture Center
100 Venture Way, Suite 201
Hadley, MA 01035-9450
Tel: (413) 545-0442
OPAM@umass.edu

Task 1: Literature Review

Prepared by: Leana Santos, Kay Wille

Problem Statement

Concrete foundations are made of Portland cement concrete (PCC), which comprises three main materials: Portland cement, aggregate (coarse and fine), and water (Figure 1). Concrete contains the element sulfur, which may be present in two forms: sulfate (SO_4^{2-}), the oxidized form of sulfur, and sulfide (S^{2-}), the most reduced form of sulfur. Portland cement contains sulfur in the form of sulfate-bearing gypsum, which is intentionally added to regulate its setting time. In typical residential construction, the total sulfur content of most unaffected concrete samples (without pyrrhotite-bearing aggregate) is expected to be between approximately 0.15% and 0.20% by weight of the hardened concrete.

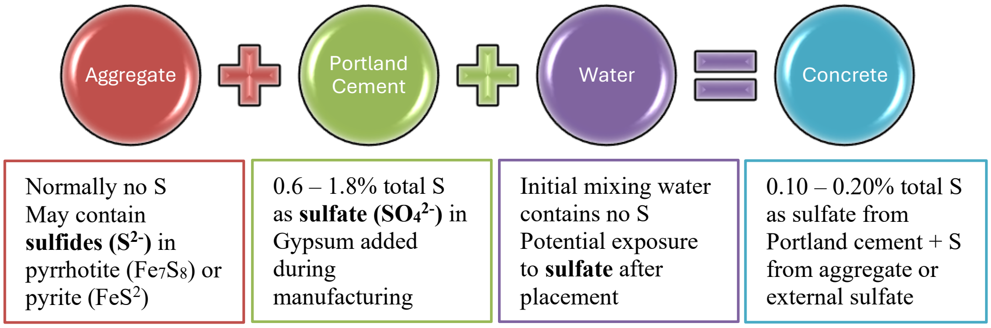

Figure 1: Overview of sulfur sources in concrete

Aggregate is a primary constituent material of cement concrete, playing a crucial role in the mix design formulations that determine concrete performance, structural capacity, and long-term durability. However, aggregates containing reactive iron-sulfide minerals, such as pyrrhotite ($Fe_{1-x}S$ where x=0-0.125) or pyrite (FeS_2), can cause premature deterioration and failure of cement concrete. The oxidation of these minerals in the presence of oxygen and water results in the formation of secondary products, releasing sulfuric acid and forming expansive minerals, both of which damage the concrete. Elevated concentrations of sulfur in concrete can indicate the potential presence of these sulfide-bearing minerals in the aggregates. Currently, no minimum acceptable level of pyrrhotite has been established. The deterioration process can start subtly in the form of interior hairline cracks and may take between 10 to 30 years to become visible, ultimately rendering the concrete structurally unsound and the damage irreversible. The role of additional factors, such as concrete quality, humidity, and other construction-related factors, is currently not fully understood.

Thousands of homes, in Northeastern Connecticut and Southwestern Massachusetts are at risk of potential foundation failure due to pyrrhotite in concrete produced between 1983 and a few years agao, using aggregate from at least one local quarry located in Willington, CT.

On December 31, 2019, a Massachusetts committee comprising legislators, technical experts, and industry members published the Final Report of the Special Commission to Study the Financial and Economic Impacts of Crumbling Concrete Foundations due to the Presence of Pyrrhotite. The report underscores the significant issue of concrete deterioration caused by pyrrhotite in the region.

Study Objectives

The objectives of this literature review are to:

- Identify and describe available experimental methods that provide qualitative (presence/absence) or quantitative (exact concentration) data on sulfur and its subspecies in solid materials.
- Evaluate the accuracy, precision, and detection limit of each testing method for aggregate materials.
- Assess the overall feasibility of implementing these testing methods for routine aggregate analysis in concrete construction projects in Massachusetts.

Method Overview

There are two primary approaches to evaluate the potential impact of pyrrhotite presence in concrete aggregate. The first approach involves measuring the total content of pyrrhotite (or a proxy, such as the sulfur or sulfide content). The second approach focuses on assessing reactivity by inducing and monitoring oxidation reactions, such as measuring the consumed oxygen or the concentration of released sulfates.

Total content-based methods typically utilize a combination of experimental techniques targeting specific chemical or mineral species, as illustrated in Figure 2. Given the legislative mandate for the quantitative determination of total sulfur and pyrrhotite in aggregate, this report focuses on content-based rather than reactivity-based methods. These methods are categorized into three distinct groups based on their capabilities and limitations in determining sulfur concentration, oxidation state, and mineralogy.

Additionally, at the end of the report, information about electrochemical accelerated testing is provided, which is an emerging and promising test methodology for evaluating the initiation and progression of damage in concrete with pyrrhotite-containing aggregates.

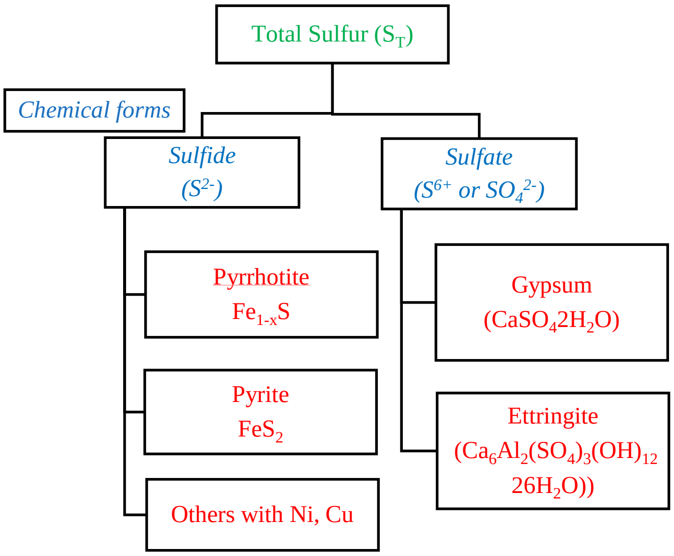

Identify with (qualitative)	Measure with (quantitative)
	Elemental analyzer X-ray fluorescence (XRF)
X-ray Photoelectron Spectroscopy (XPS)	Wavelength Dispersive XRF (sulfide and sulfate) Gravimetric analysis (sulfate only)
Thermomagnetic analysis (pyrrhotite only) Raman X-ray Diffraction (XRD) all minerals above 1 wt.% Electron Microscopy	Optical Microscopy (semi-quantitative) XRD (with imitations)

Figure 2: Overview of experimental techniques for evaluating reactive sulfur species in concrete and aggregate

Category 1: Quantification of Total Sulfur Content in Concrete and Aggregates

X-Ray Fluorescence Spectroscopy (XRF):

X-Ray Fluorescence (XRF) is a non-destructive analytical technique used to determine the bulk elemental composition of materials, including sulfur, in both concrete and aggregates. XRF is particularly well-suited for fast screening applications when the specific analytes of interest are unknown. However, its accuracy and limit of detection (LOD) are lower than those of conventional laboratory-based atomic spectrometric techniques [1]. XRF has been employed to analyze the elemental composition of various environmental, geological, and biological samples, including soils, sediments, plants, air dust, food, and archaeological and historical objects. Despite its wide range of applications, classical XRF faces significant limitations in directly analyzing liquid samples due to high background noise from scattering on water molecules and low X-ray penetration depth. [2].

There are two forms of XRF: Wavelength Dispersive (WDXRF) and Energy Dispersive (EDXRF). WDXRF instruments are laboratory-grade, higher-cost and higher-precision instruments, while EDXRF instruments are handheld and portable but have limitations in detecting and accurately analyzing a broader range of elements. Elemental quantitative analysis of samples with WDXRF may take from 5 to 25 minutes, depending on the desired detection limit and accuracy. In contrast, EDXRF analysis typically takes between 30 seconds and 2 min. Figure 3 shows the two forms of XRF equipment available in the UConn laboratories for testing.

Figure 3: WDXRF (left) and EDXRF (right) instruments available in the UConn laboratories

Sample preparation for XRF analysis can range from none (as is analysis, especially for handheld instruments) to preparation of pressed pellets (using a hydraulic press) or fused beads (using a fusion machine) for particulate materials such as aggregate and concrete. The preparation of fused beads is often considered the industry standard in terms of precision and accuracy; however, this requires heating the material up to 1250°C, which results in off-gassing of sulfide in the form of H_2S gas, affecting the sulfur measurement. Therefore, the UConn team only employs a hydraulic press for sample preparation in both WDXRF and EDXRF analyses.

The principle of XRF is that every chemical element emits a characteristic secondary X-ray spectrum called the fluorescent spectrum when irradiated with high energy X-rays. The intensity of the XRF peaks is proportional to the elemental concentration, a principle used to generate calibration curves for quantitative analysis of each element.

WDXRF instruments measure a broader range of elements (Beryllium to Uranium) compared to EDXRF (Sodium to Uranium or Magnesium to Uranium, depending on the instrument). Light elements, including sulfur, are more challenging to detect and accurately measure using EDXRF. There is no universal detection limit for XRF instruments, as detection depends on the composition of the material, a phenomenon called the matrix effect, where the sample's nature affects the penetration depth and the scattering of X-ray photons [1, 2]. Matrix effects may necessitate the development of material-specific calibrations in addition to the standard calibrations provided with the instruments.

In addition to matrix effects, the form of the element present in the material may affect quantitative analysis. Specifically, for sulfur, quantitative analysis depends on the oxidation state of the material (this will be further discussed in category 2 methods). For both WDXRF and EDXRF, the calibration for quantitative analysis of total sulfur built into the instruments is performed using a sulfate-based standard, which means that these ready-made calibrations cannot accurately quantify total sulfur in sulfide-bearing materials such as pyrrhotite-based aggregates. In general, sulfide concentrations are underestimated when using sulfate-based calibrations from EDXRF instruments. It is possible to develop custom calibrations for an EDXRF instrument; however, this assumes a uniform matrix and only a single sulfur species (e.g., sulfide) present at a time. This possibility has not yet been investigated, to our knowledge.

For WDXRF, the difference in XRF response between sulfide and sulfate may be used to determine the relative concentrations of the two species, a method that will be further discussed in Category 2.

WDXRF instruments are generally available in both academic and commercial labs; the latter typically utilize fused bead methods to determine the elemental composition of particulate materials. ASTM has developed an array of WD-XRF-based methods specific to the material being analyzed and the target analyte. Two of the more general methods are ASTM E1621-22 [3] and E1172-22 [4].

Infrared Combustion Analysis:

Total sulfur determination in refractory materials, also known as elemental analysis, involves combustion of the sample at 1150-1550°C in an oxygen-rich environment. During this process, sulfur in the sample is converted to sulfur dioxide (SO_3), which is then measured using an infrared (IR) detector. Other detection methods, such as titration and ultraviolet spectroscopy, are also available but not applicable for aggregate materials.

Modern combustion instruments require the use of combustion accelerators to achieve complete sulfur recovery in refractory samples. Additionally, material characteristics such as water content and decomposition temperature may limit the analysis to specific types of combustion instrument furnaces. This can be problematic when multiple matrices, including those with organic constituents, moisture, or crystalline water, need to be analyzed for sulfur content [5]. ASTM method D4239-18e1 [6] is the closest method applicable to the analysis of aggregate samples and is currently adopted by the UConn team (combustion method A at 1450°C). Method D5016-16 is similar but prescribes a temperature of 1450°C for coal and coke ash products [7].

In terms of sample preparation, both ASTM methods prescribe grinding the material to the No. 60 U.S. sieve (250 μm), while other applications may require further grinding to 150 μm. The UConn team conducted a sensitivity analysis and found that the 250 μm particle size was sufficient to completely combust pyrrhotite in aggregate and concrete materials. The analysis time is two minutes. The accuracy of the method using this sample preparation has been observed to be in the range of 0.01-4.41 standard error. When the standard error exceeds 5%, further samples are analyzed to determine the source of the error.

Category 2: Determination of Oxidation States of Sulfur in Concrete and Aggregates

Wavelength Dispersive X-ray Fluorescence (WDXRF):

Wavelength Dispersive X-ray Fluorescence (WD-XRF) has been previously used to determine sulfide concentrations in sulfide ores [8, 9] and artificial mixtures of sulfur species [10-13]. WD-XRF, in combination with total sulfur elemental analysis, can determine the concentrations of sulfides and sulfates in concrete. The method relies on the fact that the oxidation state of sulfur influences the location and intensity of the characteristic XRF peaks of the element (Figure 4). This phenomenon can be used to develop calibration curves that relate the ratio of sulfate to total sulfur ($\frac{S^{6+}}{S_T}$) and sulfide to total sulfur ($\frac{S^{2-}}{S_T}$) to the ratio of the three characteristic X-ray peaks, $\frac{SK\beta}{SKa}$ and$\frac{SK\beta\prime}{SK\beta}$.

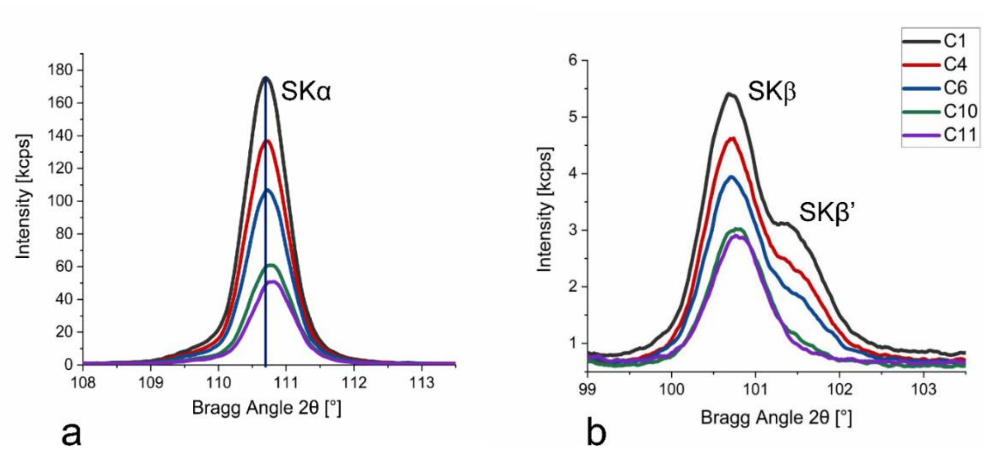

Figure 4: X-ray fluorescence spectra of selected calibration samples simulating portland cement (C1- 100% S^{6+} through C11 – 0% S^{6+} or 100% S^{2}) in the two-theta range of SKα (a) and SKβ (b)

Santos et al. [10] provide a detailed description of the method and the mathematical approach to developing rational calibration curves. They determined the sulfate weight percentage of 10 concrete samples from CT foundations with total sulfur ranging from 0.17 to 1.23 % by weight, reporting relative errors from 2.3% to 8.1% (depending on the ratio used), compared to gravimetric analysis results. The sulfide weight percentage was then determined by subtracting the sulfate percentage by weight from the total sulfur. The pyrrhotite content may be estimated using the stoichiometric ratio of 39.6%, based on the ideal formula Fe_7S_8; however, this assumes that this is the only form of sulfide in the material. Distinguishing between pyrite, pyrrhotite, or other forms of iron sulfide is not possible using this method.

Gravimetric Analysis (GA):

Gravimetric analysis (GA) analyzes sulfur in the form of sulfate in solution by precipitating it as the insoluble barium sulfate ($BaSO_4$) salt. The precipitate is isolated via filtration and combustion and its mass is used to determine the sulfur as sulfate content in the original sample. For solid materials, sulfate must first be released into solution using an acid extraction method. Since GA analysis targets the precipitation of sulfate species, sulfide cannot be measured using this method unless an oxidation step is introduced into the release process, using a strong oxidant such as H_2O_2 or $NaClO_4$.

There is no ASTM method for gravimetric analysis, but the Tex-620-J method [14] was adapted by the UConn team to measure sulfate content in concrete materials. The method involves heating a DI-water suspension to near boiling and adding concentrated HCl until the pH decreases to 2, releasing all sulfate into solution.

While the procedure is labor-intensive and time-consuming (two days are required to complete the process), requiring meticulous handling and processing, it is both reliable and straightforward. Santos et al. [10] compared the sulfate concentration of concrete samples determined using gravimetric analysis to those obtained using their developed WDXRF method. Both methods showed good agreement, as demonstrated in Figure 5. The authors reported an absolute difference in the $\frac{S^{6+}}{S_T}$ ratio between 0.00 and 0.03 for their developed rational fit. The UConn team has not attempted to determine total sulfur by adding an oxidation step to the release process.

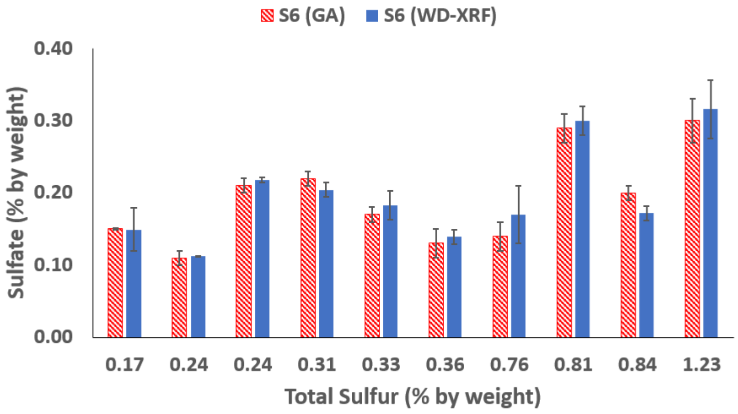

Figure 5: Comparison of averaged S^{6+} measured by Gravimetric Analysis (GA) and S^{6+} measured by WD-XRF – x-axis values indicate the total sulfur concentration of the sample.

Limitations of the GA analysis include interference from other substances that form insoluble compounds with barium or affect the oxidation and precipitation steps, which can impact accuracy.

Ion Chromatography (IC):

Ion Chromatography (IC) can be used to separate and quantify different sulfur species in solution, including sulfate, after acid digestion or extraction from the concrete or aggregate sample. Poznic et al. [15] proposed an ion chromatography method to determine chloride and sulfate concentrations in cement. This technique identifies sulfur species in cement following a two-step sample preparation procedure. The accuracy of the method was validated by analyzing a certified standard reference material (SRM), with a relative standard deviation of 0.56% for sulfur. A report by the Texas Transportation Institute, comparing GA with Ion Chromatography (described below), concluded that IC is preferred in terms of accuracy and precision when analyzing sulfate in solution and aqueous extracts.

IC is highly sensitive and capable of detecting low concentrations of ions, including sulfate ions, even in complex mixtures. However, some limitations of this technique include: (1) the preparation of samples can be labor-intensive and requires meticulous handling to avoid contamination, (2) IC systems are expensive, and (3) the technique requires trained personnel to operate the equipment and accurately interpret the results. The UConn team currently uses IC extensively to determine the reaction products of pyrite and pyrrhotite oxidation in controlled oxidation experiments; an example of a chromatogram with various sulfur oxidation products is shown in Figure 6.

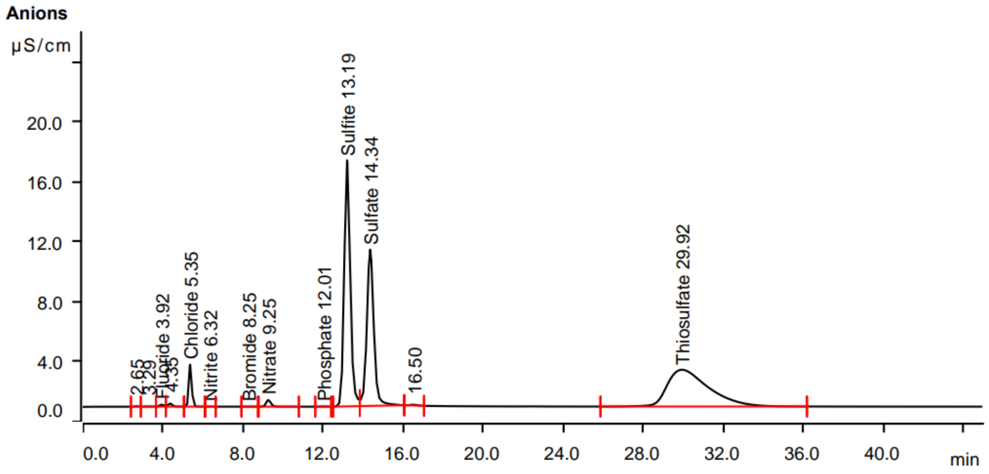

Figure 6: Ion chromatography results showing the reaction products of pyrite oxidation in controlled experiments performed by the UConn research team

Category 3: Determination of Sulfur Minerals Forms in Concrete and Aggregates

X-ray Diffraction (XRD):

X-ray diffraction (XRD) is a non-destructive technique used to analyze the structure of materials, primarily by identifying the crystalline phases present in samples through their crystal structures. This technique is particularly useful for understanding the form of sulfur present in aggregates, including sulfur-bearing minerals like pyrrhotite or pyrite. XRD can be performed in two ways: (1) qualitative XRD and (2) quantitative XRD. Minerals are identified by comparing peaks in an experimental spectrum with a database of known minerals. An example of the XRD pattern of pyrrhotite synthesized in the lab is shown in Figure 7.

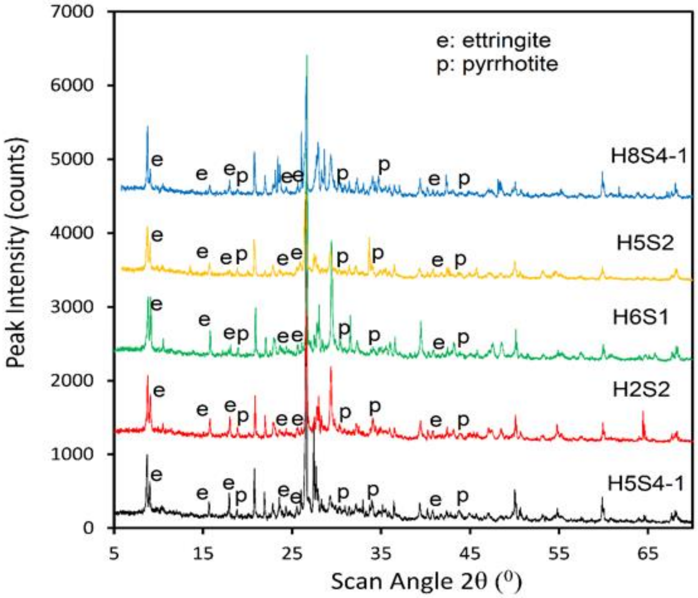

Figure 7: XRD pattern of concrete samples done by the UConn research team

The sample preparation procedures differ depending on the type of analysis. Both methods require the samples to be finely ground, homogenized, and mounted on a sample holder. However, for quantitative XRD, an internal standard must be added to quantify the phases accurately, and a finer particle size is preferable to mitigate micro-absorption phenomena.

XRD requires only a minimal amount of sample (approximately 1 g), and the sample running time is typically around 30-60 minutes, depending on the instrument and the desired spectrum quality. XRD limitations include:

- A detection limit set at 2 to 5% by mass [16]; depending on the sample matrix and experimental conditions, the limit can be as low as 0.5-1%.

- Only highly crystalline materials can be analyzed; disordered and amorphous phases are not detected.
- Extensive training is required to process the spectrum, especially for quantitative analysis.

To reduce the detection limit in XRD analysis and enhance the detection of minor phases, it is essential to optimize sample preparation, increase counting times, use advanced instrumentation, reduce background noise, apply peak enhancement techniques, and utilize advanced data processing methods. These strategies collectively improve the sensitivity and accuracy of XRD measurements, enabling the detection of phases present in lower concentrations.

Researchers have used XRD to determine the presence of pyrrhotite in aggregates. For instance, Jana [17] utilized this technique to analyze the composition of aggregates collected from a local quarry in Connecticut, USA.

Petrographic Analysis:

Petrographic analysis involves the microscopic examination of rocks and minerals to determine their composition, texture, and structure. This technique utilizes polarizing microscopes to study thin sections of rock samples, either thin-cut and prepared to a thickness of about 30 micrometers, or prepared as a flat, polished slab of concrete Petrographic analysis is particularly useful for detecting and characterizing sulfide minerals, such as pyrite and pyrrhotite, in rock and aggregate samples [18]. Minerals are identified based on their optical characteristics, aiding in the determination of the type, size, shape, and spatial distribution of minerals within the rock. Quantitative analysis by volume is performed by counting the number of a certain type of particle identified across the area of the sample.

The American Society for Testing and Materials (ASTM) has developed standard C295-19, outlining the procedure for the petrographic examination of aggregate samples intended for use in concrete production [19].

Petrographic analysis for aggregates is widely available through commercial labs, however, it is generally time-consuming and costly.

Thermomagnetic Testing:

Geiss and Gourley [20] developed a semi-quantitative method to identify pyrrhotite using its thermomagnetic properties. Their method measures the evolution in magnetic susceptibility (χ) as the material is heated between room temperature and 700°C. When the temperature reaches the Curie temperature, i.e., the temperature at which the structure and thus the magnetic properties of pyrrhotite change, χ drops abruptly, with the magnitude of the decrease depending on the amount of pyrrhotite in the sample. The method is semi-quantitative; when magnetic pyrrhotite is detected, the total concentration of sulfur measured via combustion is translated to pyrrhotite via stoichiometry [20]. Using this approach, this method can detect pyrrhotite concentrations as low as 0.1% [20]. One of the main limitations of this methodology is that the method's sensitivity depends on the magnetic susceptibility of the pyrrhotite, which can vary depending on its structure, i.e., not all pyrrhotite crystal forms have magnetic properties.

Scanning Electron Microscopy – Energy Dispersive Spectroscopy (SEM-EDS):

SEM-EDS combines imaging at the micro-level (typical resolution is 1-100 µm) with elemental analysis, enabling the visualization of sulfur-bearing phases and determination of their composition, an example is shown in Figure 5. This method provides both qualitative and semi-quantitative information on sulfur distribution. SEM/EDS is routinely used to identify pyrrhotite by its unique Fe/S ratios, though it currently cannot accurately quantify the 4C/5C structures of pyrrhotite due to similar ratios [21].

Multani et al. [21] have highlighted that current mineralogical programs employ quantitative X-ray diffraction (XRD) in conjunction with chemical assays and QEMSCAN/MLA to determine the 4C/5C structure ratio and total pyrrhotite content. However, when dealing with mineral associations or samples containing less than 5% wt. pyrrhotite, the quantification of superstructures is challenging and requires the use of SEM for more accurate analysis.

Some limitations associated with this technique include:

1. Fine Grain Differentiation: Difficulty in differentiating within fine grain sizes.
2. Technician Expertise: Results are dependent on the technician's expertise
3. Tedious Nature: The method is labor-intensive and time-consuming.

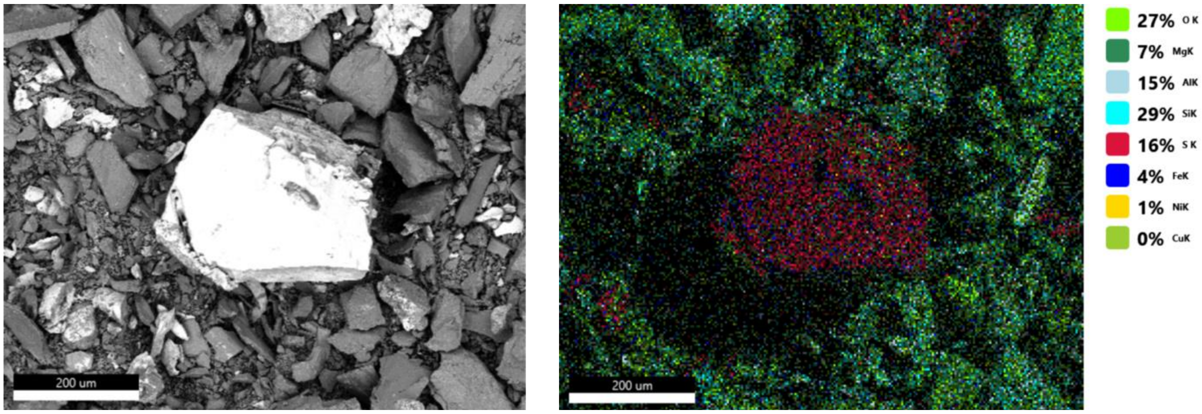

Figure 8: SEM-EDS mapping results on sulfur-rich aggregate

X-ray Photoelectron Spectroscopy (XPS):

X-ray Photoelectron Spectroscopy (XPS) is an analytical technique used to study the surface chemistry of materials. XPS is based on the photoelectric effect, where X-rays irradiate a material, causing the emission of photoelectrons. By analyzing the binding energy shifts, XPS can identify the chemical states of elements, indicating oxidation states, chemical bonding environments, and other electronic structures.

Some of the advantages of XPS include:

1. High Sensitivity: It provides quantitative information about the elemental composition of the surface (typically the top 1-10 nm).
2. Non-Destructive: Preserves the sample for further analysis.
3. Chemical State Analysis: Can identify various chemical states and bonding environments.

However, this technique also has some limitations:

1. Surface Analysis: It analyzes only the surface of the sample, which may not be representative of the bulk material.
2. High Vacuum Requirement: Analysis must be performed in a high vacuum environment.
3. Special Preparation for Non-Conductive Samples: Non-conductive samples may require special sample preparation to prevent charging effects.

XPS has been used to characterize and quantify iron sulfides in concrete. According to Chinchón-Paya et al. [22], XPS can differentiate between sulfur species even at low levels of pyrrhotite. Quantification requires a standard addition method to generate matrix-specific spectra at known concentrations of pyrrhotite. Given that XPS is a time-consuming method, requiring several hours per sample, and that the equipment is only available in specialized academic facilities, it is not a viable method for routine characterization of materials.

Micro X-ray Fluorescence (µXRF):

Micro-XRF is a method used for elemental mapping of samples, enabling the characterization and quantification of iron sulfides found in aggregates, although it does not differentiate between pyrite and pyrrhotite minerals [22]. Researchers have used Micro-XRF to study concrete core samples containing aggregates with iron sulfide minerals, employing elemental chemical distribution images to identify mineral phases and conducting quantitative analysis through image analysis.

Micro-XRF allows for elemental mapping of areas up to 15 cm with a minimum beam size of 20 µm. It can distinguish sulfide types and detect sulfur concentrations as low as 0.1% by mass if the aggregates contain pyrrhotite. The researchers highlighted that larger samples can be analyzed using micro-XRF compared to SEM-EDX, making micro-XRF particularly suitable for concrete durability studies.

Other testing techniques for quantifying sulfur and its specific forms in concrete are currently being evaluated in research laboratories worldwide, although their results have yet to be published [23]. These techniques include, but are not limited to, Raman Spectroscopy, Auger Electron Spectroscopy, Laser-Induced Breakdown Spectroscopy (LIBS), and Nuclear Magnetic Resonance Spectroscopy. However, the potential for application of these techniques for routine characterization of aggregates is currently low.

Summary of content-based methods

Table 1 summarizes the main findings of the content-based methods.

Table 1: Overview of Sulfur Analysis Methods and Limitations

	Matrix	Sample preparation	Quantitative	Detection Limit	Commercially available?
Category 1: Total S					
WDXRF	Solid	Pellet/ beads	Yes	1-5 ppm	Yes
EDXRF	Solid	Pellet/ none	Yes	45 ppm	Yes
Infrared Combustion	Solid	Pulverization	Yes	0.5-1 ppm	Yes
Category 2: Sulfur Oxidation States					
WDXRF	Solid	Pellet	Yes	0.25%	Yes
Gravimetric analysis	Liquid	Acid extraction for solids	Yes	0.1% to 1%	Yes
Ion Chromatography	Liquid	Acid extraction for solids	Yes	0.1 to 1 ppm	Yes
Category 3: Sulfur minerals					
XRD	Solid	Pulverization	Semi	n.a.	Yes (limited)
Petrography	Solid	Polished section	Semi	n.a.	Yes
Thermomagnetic	Solid	Pulverization	Semi	0.1%	No
SEM/EDS	Solid	Pulverization and coating or thin section	No	0.1% to 1%	No
XPS	Solid	Pulverization	No/Semi	0.1 to 1 atomic %	No
µXRF	Solid	Polished section	No	0.1%	No

Electrochemical Accelerated Testing

Electrochemical accelerated testing is an emerging method that has recently gained attention for studying concrete deterioration caused by the presence of iron sulfide-containing aggregates, especially in the form of pyrrhotite [24-27]. This method is based on the principles of NT BUILD 492 1999 [28] and ASTM C1202-22 [29], with modifications to the test setup (see Figure 9) and electrolytes. The process involves driving chloride ions (Cl^-) into a lab-cast or field-cored cylindrical concrete specimen by applying voltage to both end faces of the specimen in contact with the electrolytes. The chloride ions increase the specimen's conductivity, while the applied voltage accelerates the oxidation of pyrrhotite, leading to deterioration within days or weeks, depending on factors such as amount of pyrrhotite, voltage magnitude, electrolyte type, and aggregate sizes. Studies using concrete specimens without pyrrhotite have consistently shown no deterioration, underscoring the connection between pyrrhotite and damage in the concrete [24, 25].

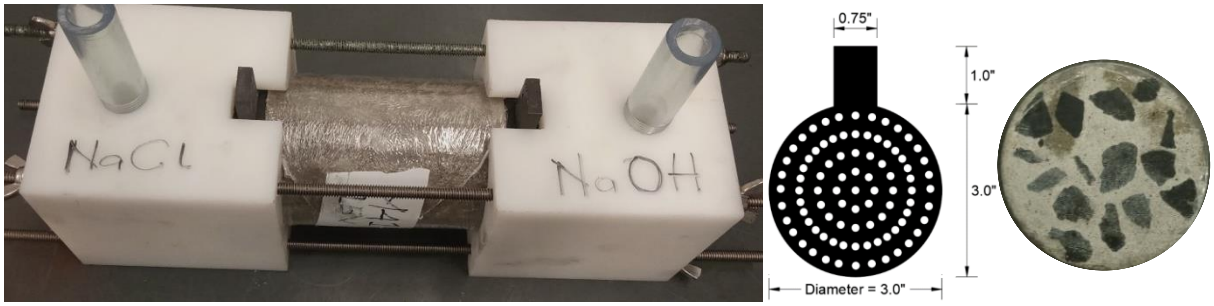

Figure 9: Accelerated setup with wrapped concrete sample, design of electrode and ground cylinder face.

Recent studies have integrated this method with destructive and non-destructive testing techniques for evaluating damage [24, 27]. In the most recent study by Ojo et al. [24], resonance frequency testing was used in combination with crack length measurement at 7-day intervals to track changes in the dynamic elastic modulus ($E_{\mathrm{dyn,c}}$) of the specimens as deterioration developed and progressed. The conceptual steps of the electrochemical acceleration process utilized in [24] are shown in Figure 10 below.

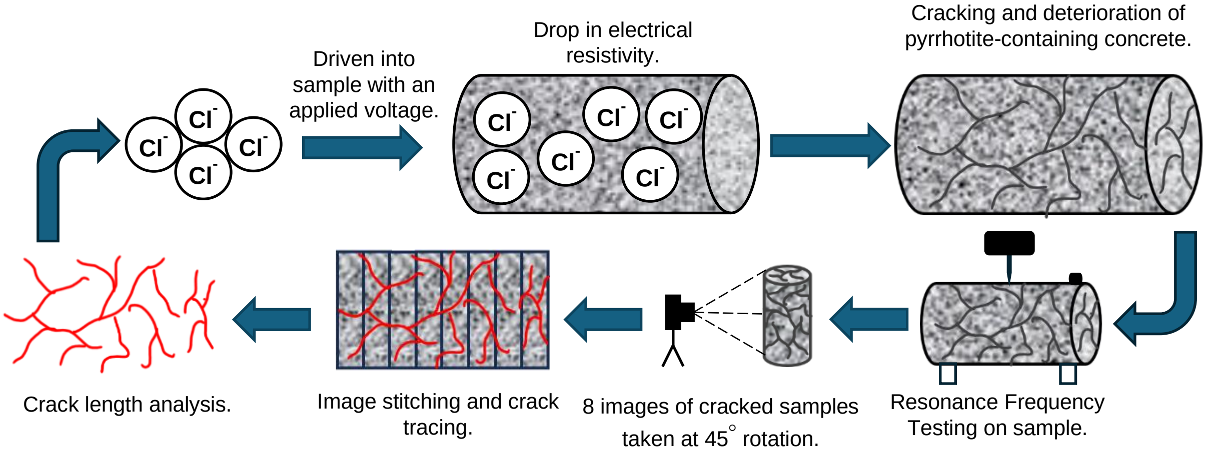

Figure 10: Time-dependent steps of electrochemical accelerated testing and non-destructive damage evaluation

During testing, specimens typically exhibit significant deterioration, as shown in Figure 11. Common signs of damage include reddish-brown discoloration, extensive cracking, and map cracking on the sample surface, along with concrete pop-outs. These signs are consistent with deterioration patterns observed in concrete containing pyrrhotite-bearing aggregates in the field. However, a challenge with this method is the dissolution of the matrix on the sodium hydroxide (NaOH) end face of the concrete specimen due to the highly acidic conditions that develop at that end of the test cell as testing progresses.

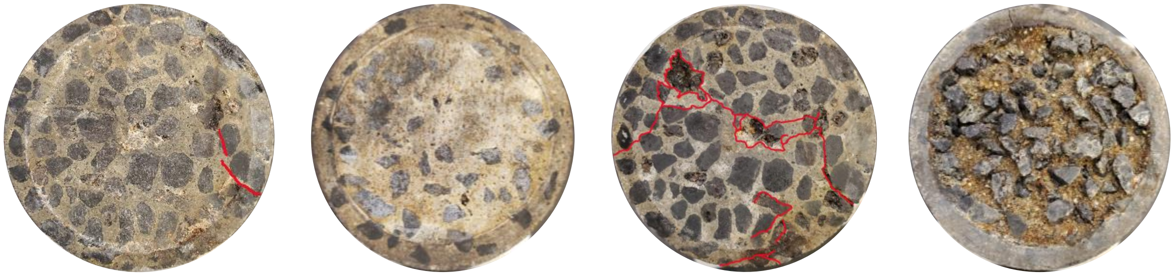

(a) NaCl face, 14 days *(b) NaOH face, 14 days* *(c) NaCl face, 77 days* *(d) NaOH face, 77 days*

(e) Body of specimen, 14 days *(f) Body of specimen, 77 days*

Figure 11: Tested specimen with traced cracking (NaCl – NaOH, 45V).

The progression of cracks on the sodium chloride (NaCl) end face and body of a tested specimen containing pyrrhotite bearing aggregates at 14, 35, 56, and 77 days are shown in Figure 12, illustrating surface crack evolution over time. The number of cracks and total crack length increased with exposure duration.

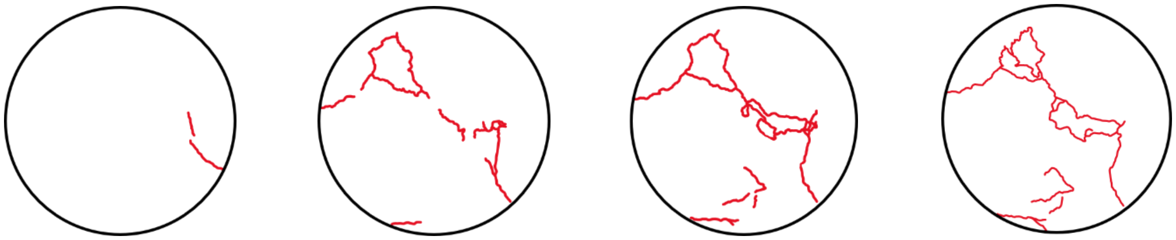

(a) NaCl face, 14 days *(b) NaCl face, 35 days* *(c) NaCl face, 56 days* *(d) NaCl face, 77 days*

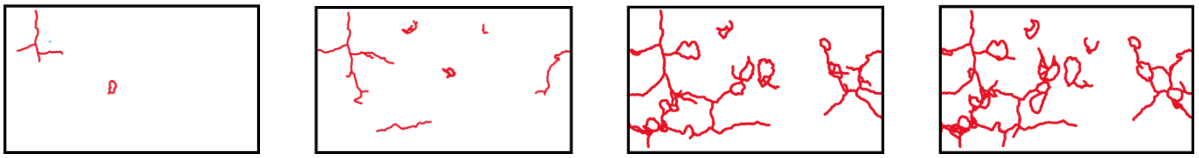

(e) Body, 14 days *(f) Body, 35 days* *(g) Body, 56 days* *(h) Body, 77 days*

Figure 12: Exposure time-dependent traced crack evolution of tested specimen (NaCl – NaOH, 45V).

Some of the benefits and limitations of the electrochemical acceleration method are highlighted below.

Benefits:

1. The accelerated deterioration test provides a controlled environment to study chemical reactions, oxidation rates, and the impact of concrete quality on pyrrhotite oxidation.
2. The method aids in developing a robust prediction model and risk assessment framework for evaluating concrete foundations with iron-sulfide aggregates.
3. Techniques like crack tracing and RF testing provide valuable, nondestructive methods for assessing the onset and progress of deterioration.
4. The method shows similar damage patterns to early-stage deterioration observed in field samples, making it a useful tool for predicting long-term damage.
5. The electrochemical method effectively accelerates deterioration in lab and field samples containing pyrrhotite, highlighting its relevance for such studies.

Limitations:

1. More comprehensive studies are needed to generate data that ensures statistical confidence in the similarity between lab-based and field-based deterioration.
2. The influence of aggregate size on deterioration rates requires further investigation to fully understand its impact.
3. The method currently shows deterioration over shorter durations; longer-term studies are necessary to assess damage over extended periods.

4. The method’s reliance on higher applied voltage may not fully replicate natural field conditions, indicating the need for further studies to better align the testing parameters with real-world scenarios.
5. Further studies are required to investigate the best electrolyte conditions for the method. Conventional approaches using NT BUILD 492 1999 [28] and ASTM C1202-22 [29] result in dissolution of the NaOH-connected end face, while replacing NaOH with NaCl leads to significant heating of the sample after a few weeks.

Overall, the electrochemical acceleration method demonstrates significant potential for expediting the deterioration of concrete specimens containing iron sulfide-bearing aggregates. It provides valuable insights through nondestructive evaluation techniques. However, further development is necessary to refine the method. Additional research is essential to obtain statistically robust results, particularly in correlating lab-based deterioration with field conditions, before this method can be widely accepted as a standard for evaluating concrete deterioration in practical applications. Furthermore, the use of microstructural investigation methods, such as SEM and XRD, will aid obtaining valuable insight in the formation and growth of pyrrhotite oxidation-related reaction products in electrochemically accelerated concrete specimens.

Future Direction: Next Steps

The next step involves initiating the study and testing of concrete mix design mitigation methods to evaluate their effectiveness in preventing or slowing the deterioration of cement concrete containing pyrrhotite-reactive minerals. This task will begin with a comprehensive review of relevant literature to gather information on available and potentially successful mitigation methods. Following this, an accelerated testing environment will be designed and set up to simulate long-term effects in a shorter timeframe, allowing for a quicker evaluation of the mitigation methods.

Updates: *Preliminary laboratory tests will be conducted to assess the effectiveness of mitigation strategies. Data collected from these tests will be recorded and analyzed to identify trends and determine the most promising methods. Progress and findings will be regularly updated and discussed during virtual meetings with the project champion and technical representative.*

Deliverables: *A written summary will be provided, detailing the available and potentially successful mitigation methods, along with preliminary data and analysis obtained from the initial laboratory tests.*

References

[1] Hou, Xiandeng, et al. “Recent Advances in Portable X-Ray Fluorescence Spectrometry.” *Applied Spectroscopy Reviews*, vol. 39, no. 1, 31 Dec. 2004, pp. 1–25, doi:10.1081/asr-120028867.

[2] Klisińska-Kopacz, Anna. “Chapter 17 - X-Ray Fluorescence Spectroscopy.” *Non-Destructive Material Characterization Methods*, Elsevier, pp. 487–523, Accessed 2024.

[3] ASTM E1621-22: Standard Guide for Elemental Analysis by Wavelength Dispersive X-Ray Fluorescence Spectrometry

[4] E1172-22: Standard Practice for Describing and Specifying a Wavelength Dispersive X-ray Spectrometer

[5] Darling, Adam, et al, 2018. “Determination of Total Sulfur in Refractory Samples: Comparing Various Elemental Analysis Techniques” PITTCON 2018, February 26-March 1, Orlando, Florida.

[6] ASTM D4239-18e1: Standard Test Method for Sulfur in the Analysis Sample of Coal and Coke Using High-Temperature Tube Furnace Combustion

[7] ASTM D5016 – 16: Standard Test Method for Total Sulfur in Coal and Coke Combustion Residues Using a High-Temperature Tube Furnace Combustion Method with Infrared Absorption

[8] Chubarov, Victor, et al. “X-Ray Fluorescence Determination of Sulfur Chemical State in Sulfide Ores: Sulfur Chemical State Determination by WDXRF Analysis.” *X-Ray Spectrometry*, vol. 45, no. 6, 2016, pp. 352–56, https://doi.org/10.1002/xrs.2712.

[9] Chubarov, Victor, et al. “Determination of Sulfide and Total Sulfur in Ore by Wavelength-Dispersive X-Ray Fluorescence.” *Analytical Letters*, vol. 49, no. 13, 2016, pp. 2099–107, https://doi.org/10.1080/00032719.2015.1136933.

[10] Santos, L et al. “Application of X-ray principles to quantify sulfur oxidation states in concrete”, *Spectroscopy Letters,* 2024, DOI: 10.1080/00387010.2024.2361709

[11] Cruz-Hernandez, Yusniel, et al. “Wavelength Dispersive X-Ray Fluorescence Method to Estimate the Oxidation Reaction Progress of Sulfide Minerals in Concrete.” *Spectrochimica Acta Part B: Atomic Spectroscopy*, vol. 172, 2020, p. 105949, https://doi.org/10.1016/j.sab.2020.105949.

[12] Uhlig, S., et al. “Quantitative Analysis of Sulphides and Sulphates by WD-XRF: Capability and Constraints.” *X-Ray Spectrometry*, vol. 45, no. 3, 2016, pp. 133–37, https://doi.org/10.1002/xrs.2679.

[13] Pechishchev, I. V., et al. *Determination of Sulfur Content in Various Oxidation States by WD – XRF*. 2022, p. 050027, https://doi.org/10.1063/5.0088660.

[14] Tex-620-J: Determining Chloride and Sulfate Content in Soils

[15] Poznic, Marjeta, et al. “Ion Chromatography Determination of Chloride and Sulphate in Cement.” *Cement and Concrete Research*, vol. 29, no. 3, Mar. 1999, pp. 441–443, doi:10.1016/s0008-8846(98)00234-8.

[16] Janzen, Michael P, et al. “Pyrrhotite Reaction Kinetics: Reaction Rates for Oxidation by Oxygen, Ferric Iron, and for Nonoxidative Dissolution.” *Geochimica et Cosmochimica Acta*, vol. 64, no. 9, May 2000, pp. 1511–1522, doi:10.1016/s0016-7037(99)00421-4.

[17] Jana, Dipayan. “Pyrrhotite Epidemic in Eastern Connecticut: Diagnosis and Prevention.” *ACI Materials Journal*, vol. 117, no. 1, Jan. 2020, doi:10.14359/51718059.

[18] Berrezueta, Edgar, et al. “Ore Petrography Using Optical Image Analysis: Application to Zaruma-Portovelo Deposit (Ecuador).” *Geosciences*, vol. 6, no. 2, 21 June 2016, p. 30, doi:10.3390/geosciences6020030.

[19] ASTM C295-19: Standard Guide for Petrographic Examination of Aggregates for Concrete

[20] Geiss, Christoph E., and Jonathan R. Gourley. “A Thermomagnetic Technique to Quantify the Risk of Internal Sulfur Attack Due to Pyrrhotite.” *Cement and Concrete Research*, vol. 115, Jan. 2019, pp. 1–7, doi: 10.1016/j.cemconres.2018.09.010.

[21] Multani, Ravinder S., and Kristian E. Waters. “A Review of the Physicochemical Properties and Flotation of Pyrrhotite Superstructures (4C–Fe_7S_8/ 5C–Fe_9S_{10}) in Ni-Cu Sulphide Mineral Processing.” *The Canadian Journal of Chemical Engineering*, vol. 96, no. 5, 19 Jan. 2018, pp. 1185–1206, doi:10.1002/cjce.23099.

[22] Chinchón-Payá, S., et al. “Study of Aggregate Samples with Iron Sulfides through Micro X-Ray Fluorescence (µXRF) and X-Ray Photoelectron Spectroscopy (XPS).” *Materials and Structures*, vol. 48, no. 5, 20 Dec. 2013, pp. 1285–1290, doi:10.1617/s11527-013-0233-z.

[23] Jana, Dipayan. “Preventing Pyrrhotite Damage in Concrete.” *Concrete International*, vol. 46, no. 5, pp. 42–47.

[24] M. Ojo, et al., “Electrochemical investigation of accelerated deterioration of concrete with iron-sulfide containing aggregates*”, Cement and Concrete Research*. 182 (2024).

[25] R. Castillo Araiza et al., “Electrochemical activation of oxidation of sulfide-bearing aggregates in concrete specimens”, *Cement and Concrete Research*. 170 (2023) 107186.

[26] R. Castillo Araiza, et al., “A new accelerated testing scheme to evaluate the potential oxidation reaction of sulfide-bearing aggregates in concrete specimens *Cement and Concrete Research*. 180 (2024) 107507.

[27] R. Castillo Araiza, et al., Evaluation of detrimental effects in concrete specimens due to the oxidation of sulfide-bearing aggregates after electrochemical treatment*, Construction and Building Materials*. 411 (2023).

[28] NT BUILD 492, Concrete, Mortar and Cement-Based Repair Materials: Chloride Migration Coefficient from Non-Steady-State Migration Experiments, *Nordtest Method*. (1999).

[29] C09 Committee, ASTM C1202-22, Test Method for Electrical Indication of Concretes Ability to Resist Chloride Ion Penetration, ASTM International. (2022).

Task 2: Concrete Mix Design Mitigation Methods

Prepared by: Meshach Ojo, Ana Rocha, Kay Wille

Study Objectives

During this task, the study and testing of the effectiveness of concrete mix design mitigation methods on the evolution of deterioration of cement concrete containing pyrrhotite reactive minerals were initiated. This included gathering information about available and potentially successful mitigation methods, as well as setting up the accelerating test setup and performing preliminary laboratory tests on selected parameters. The selected parameters included the impact of water to cement ratios and type of cement on the deterioration of concrete with pyrrhotite aggregates. Updates have been provided and discussed during regular virtual meetings with the project champion and technical representative, and a summary of the results are presented here.

Electrochemical Accelerated Testing

Recent studies have used the Electrochemical accelerated testing (EAT) method to expedite the deterioration of lab-cast and field-cored pyrrhotite-containing concrete specimens in the laboratory [1-3]. This method is based on the principles of NT BUILD 492:1999 [4] and ASTM C1202-22 [5], and involves driving chloride ions into the concrete specimen by applying a constant voltage across both end faces. Although EAT is still in development and requires more data to improve statistical confidence between lab-based and field-based deterioration, this method can be highly useful for testing potential mitigation strategies in a controlled environment.

Reducing the water-cement (w/c) ratio may serve as an effective mitigation strategy for both deterioration and strength retention in pyrrhotite-containing concrete. Many design codes, such as ACI and BS, recommend lowering the w/c ratio to control the ingress and transport of sulfate ions, a process that contributes to secondary stage of deterioration in pyrrhotite-containing concrete [6]. By decreasing the w/c ratio, the transport of reactive agents can be inhibited, potentially reducing the rate of deterioration. Additionally, a reduced w/c ratio enhances concrete resistance to sulfate attack by increasing its tensile strength [7]. This increased strength can directly reduce damage from localized stress. This study performed preliminary laboratory tests on affected concrete specimens with various w/c ratios to initiate the investigation of potential effective mitigation strategy.

The use of different types of cement is also being investigated as a potential strategy to mitigate the deterioration of concrete caused by the presence of pyrrhotite. Tricalcium aluminate (C_3A) is one of the main constituents of ordinary Portland cement (OPC) [8]. A high content of C_3A in Portland cement is known to reduce its resistance to sulfate attack. The interaction of C_3A with sulfates can lead to the formation of ettringite and thaumasite, both of which are associated with expansion, microcracking, and disintegration of the calcium silicate hydrate (C-S-H) structure [9].

Oilwell cements, primarily used in the exploration and production of oil and gas to secure metal casings and liners, offer a potential alternative. Class G High Sulfate Resistant (HSR) cement, with a low C_3A content (maximum 3%), is designed to enhance resistance to sulfate attack [10]. For this reason, the use of Oilwell Cement was explored with the aim of evaluating the performance of samples containing pyrrhotite aggregates when subjected to electrochemical accelerated testing. In addition, concrete samples cast with Type I White cement, which contains a lower proportion of tetracalcium aluminoferrite (C_4AF), were also examined to assess how lower C_4AF content might influence the deterioration rate of the concrete. The hydration behavior of tetracalcium aluminoferrite has similarities with that of C_3A, but due to its complex structure and the variety of hydration products formed, the exact hydration mechanism requires further validation [11].

Using the EAT method, the aim of this study was to understand how varying the w/c ratio and cement types affects the deterioration rate of pyrrhotite-containing concrete specimens in the laboratory. Damage evaluation and assessment were carried out by measuring the dynamic elastic modulus from resonance frequency testing, as well as through visual observation for signs of deterioration and cracking. These findings contribute to our understanding of pyrrhotite-containing concrete deterioration and will inform future mitigation approaches.

Materials and Methods:

Concrete cylindrical specimens were cast using cements of varying types and compositions, as detailed in

Table 1. River sand (RS) consisting of two gradations was used as fine aggregate. The first gradation (FR1) comprised aggregate particle sizes smaller than 1.18 mm (#16 US standard sieve), while the second gradation (FR2) included particle sizes larger than 1.18 mm (#16 US standard sieve) but smaller than 4.75 mm (#4 US standard sieve). Two types of coarse aggregates were used for the control and pyrrhotite-containing specimens: locally sourced non-pyrrhotite aggregates (NP) and pyrrhotite-containing aggregates (CA1) obtained from Trois-Rivières, Quebec, Canada. Both types of aggregates were prepared in two gradations: the first gradation (FR3) consisted of aggregate particle sizes larger than 4.8 mm (#4 US standard sieve) but smaller than 9.5 mm (3/8" sieve), while the second gradation (FR4) included sizes larger than 12.7 mm (1/2" sieve) but smaller than 16 mm (5/8" sieve). All aggregates and cement were pulverized (smaller than 250 µm or #60 US standard sieve) and analyzed for total sulfur (ST) percentage in accordance with ASTM D4239 [12] guidelines to determine their sulfur content. The ST percentages from the analysis were 1.18 ± 0.05% for type I/II cement, 0.04% for RS, 0.04% for NP, and 1.39 ± 0.06% for CA1.

Table 1: Percentage Chemical Composition of Cements

Type	SiO_2	Al_2O_3	Fe_2O_3	CaO	MgO	SO_3	Na_2O	K_2O
I/II	18.73	5.35	4.69	61.47	2.67	3.30	0.40	0.97

Type	C_3S	C_2S	C_3A	C_4AF	SO_3
Oil-Well	55	21	0	18	2.1
White	69	9	10	1	2.7

Concrete Mixture Design and Sample Preparations:

Several cylindrical concrete specimens were cast according to ASTM C192/C192M – 19 [12] using molds measuring 76 mm in diameter by 152 mm in length. To ensure an optimal blend of coarse and fine aggregates, the 0.45 power grading method was employed before mixing, with the results approximated into four equal gradations, as shown in Table 2. An air entraining admixture was used during casting to achieve a total air void content of 6.2%, matching values observed in field samples from petrographic analysis. A w/c ratio of 0.6 was employed as a typical value for concrete foundation samples in the field. Additionally, a w/c ratio of 0.4 was included in this study to investigate the effect of w/c ratio on the deterioration rate (Table 2).

Table 2: Weight-based mixture proportions

Cement	**Water**	**Air Entrainer**	**Fine aggregates**		**Coarse aggregate**	
			FR 1 ***($x < 1.18$) mm***	**FR 2** ***($1.18 < x < 4.8$) mm***	**FR 3** ***($4.8 < x < 9.5$) mm***	**FR 4** ***($12.7 < x < 16$) mm***
1*	0.6	0.0009	1.02	1.02	1.02	1.02
1**	0.4	0.0009	0.80	0.80	0.80	0.80

* 386.5 kg/m^3 ** 494.2 kg/m^3

The study included two types of specimens: control specimens (C1), which did not contain any pyrrhotite, and pyrrhotite-containing specimens (P5). The C1 specimens served as a baseline for comparing deterioration rates with the pyrrhotite-containing specimens during testing. The P5 specimens were cast in two sets. In the first set, only the w/c ratio differed, while all other components were kept constant. In the second set, every parameter was kept constant except for the type of cement. Two specimens were cast for each testing series to enhance the robustness of the test data and ensure reproducible results. Detailed information about all the mixtures used in this study is provided in Table 3.

Table 3: Experimental Parameters

	Specimen ID	**Height (mm)**		**Aggregate Size Fractions**				**Cement Type**	**Calc. ST (%)**	**Test period (Days)**		**Test Objective**
		1	**2**	**FR1**	**FR2**	**FR3**	**FR4**			**1**	**2**	
G1	C1 (0.6)	147	147	RS	RS	NP	NP	Type I/II	0.24	133	133	Compare deterioration rates
	P5 (0.6)	136	132	RS	RS	CA1	CA1		0.72	77	77	

	P5 (0.4)	148	147	RS	RS	CA1	CA1		0.75	140	140	under different water cement ratios
G2	P5 (OW)	127	126	RS	RS	CA1	CA1	Oil-Well	0.66	42	42	Compare deterioration rates under different cement types
	C1 (OW)	147	147	RS	RS	NP	NP		0.17	91	91	
	P5 (W)	148	149	RS	RS	CA1	CA1	White	0.70	77	63	
	C1 (W)	146	146	RS	RS	NP	NP		0.21	77	77	

The specimens were cured at room temperature (23 ± 2°C) and 95% relative humidity for 13 days. Afterward, the end faces were ground to ensure surface evenness in the test setups. The specimens were then immersed in tap water for 24 hours to increase conductivity and subsequently tested for Resonance Frequency (RF). Before placement in the setups, photos of the specimens were taken, and they were wrapped in plastic sheets, exposing only the end faces. Wrapping was done to prevent electrolyte flow across the specimen surface during testing. Finally, the specimens were assembled in the setups for electrochemical testing.

Electrochemical Testing Setup**:**

The electrochemical testing setup consisted of two cuboidal reservoirs made from high-density polyethylene sheets (HDPE), with one open face to hold the concrete specimens. Both reservoirs were fastened with stainless steel rods and held the 76 mm by 152 mm cylindrical concrete specimen between them. One reservoir was filled with a 1.7M sodium chloride (NaCl) solution, while the other contained a 0.3M sodium hydroxide (NaOH) solution. Perforated graphite sheets, machined into the shape shown in Figure 1, were used as electrodes. The electrodes were secured with rubber gaskets to prevent damage from end-bearing pressure between the specimen's end face and the HDPE sheet. All setups were connected to a switching 60V DC power source (Model 1685B, B&K Precision, California, USA) using a pair of red and black 18 AWG banana-to-alligator clip patch cords. The black patch cord linked the negative terminal of the DC source to the NaCl side, while the red patch cord linked the positive terminal to the NaOH side of the electrochemical setup.

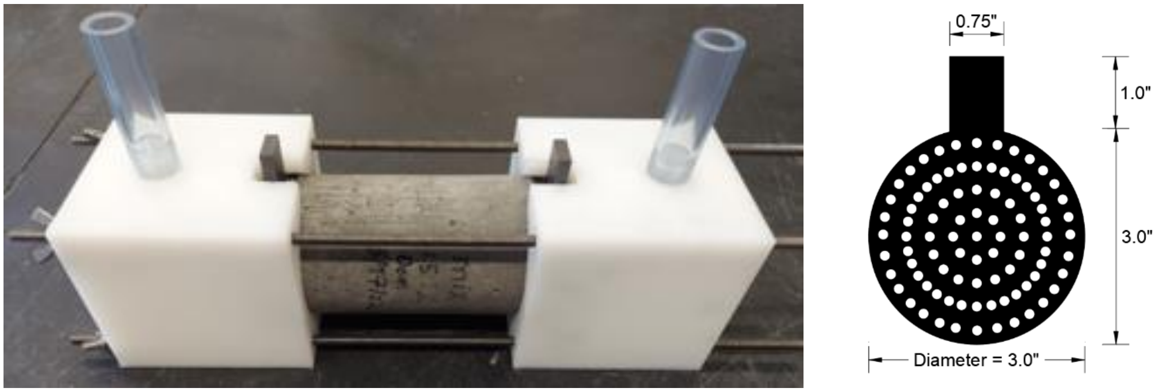

Figure 1: Electrochemical accelerated test setup (left) and perforated graphite electrode (right).

Crack Increment Monitoring:

The specimens were inspected regularly for damage and cracking before testing, and each time they were removed from the test setups for RF testing. Pictures of the specimens were taken using a Canon EOS Mark II digital camera (24.1-megapixel resolution) and subsequently analyzed on a computer for signs of cracking and deterioration. To ensure consistency in crack analysis, photographs of the end faces were taken first, followed by images of the specimen's body. The body was marked into eight equal sections, and eight pictures were captured at 45^o rotations on a rotating platform from a fixed position. The body images were then cropped and arranged side-by-side to create a continuous 2D image and provide a seamless visualization of the crack network.

Resonance Frequency Testing:

Resonance frequency (RF) testing was performed on the specimens prior to testing and at regular intervals (at least 7 days) to evaluate damage over the testing period. Testing was conducted using the transverse mode described in ASTM C215 – 19 [13] and subsequently, the dynamic elastic was calculated using the accompanying equation in [13]. The specimens were weighed, and the testing was done using the average of triplicate values obtained. After testing, the specimens were replaced in test setups, ensuring they were out of testing conditions for a maximum of 45 minutes.

Results and Discussions:

Change in Water-Cement Ratio – Group 1 (G1):

In G1, the primary objective was to compare the effect of varying the water to cement ratio on the deterioration rate of pyrrhotite-containing specimens.

Effects on Damage and Cracking:

Figure 2 shows the images of G1 specimens at 42 days and at the end of testing. After 133 days of testing, the control sample C1 (0.6) showed no visible signs of damage, either in the form of discoloration or cracking. This observation, which was consistent with findings from our previous study [1] was expected, as C1 did not contain any pyrrhotite aggregates. In contrast, P5 (0.6) and P5 (0.4) specimens presented signs of deterioration, which included reddish-brown discoloration indicative of pyrrhotite oxidation, concrete pop-outs around discolored areas (comprising paste mixed with fines), and cracking on the NaCl face and body of the specimens. Visual inspection revealed that the cracks initiated from oxidized pyrrhotite aggregates, extended into the matrix, and eventually propagated through the body of the specimen. These cracks were due to localized stresses on the concrete matrix around the aggregates resulting from expansion after severe oxidation.

The severity and extent of discoloration, pop-outs, and cracking also varied among the pyrrhotite-containing specimens in G1. P5 (0.6), which had a higher w/c ratio, exhibited more damage compared to P5 (0.4), which had a lower w/c ratio in its mixture. This observation was consistent across all time periods, starting from the first 7 days of testing. Although testing was terminated for P5 (0.6) at 77 days, the extent of damage remained more pronounced compared to P5 (0.4) at 140 days, when testing was terminated for this specimen. The higher resistance of P5 (0.4) compared to P5 (0.6) is strongly linked to the lower w/c ratio. Lower w/c ratios result in denser matrix and higher strength. While deterioration is still evident, this variation in deterioration rate demonstrates that the w/c ratio significantly affects damage, and lower w/c content can lead to prolonged service life for pyrrhotite-containing concrete structures.

P5 (0.6), NaCl face, 42 days P5 (0.6), NaCl face, 77 days

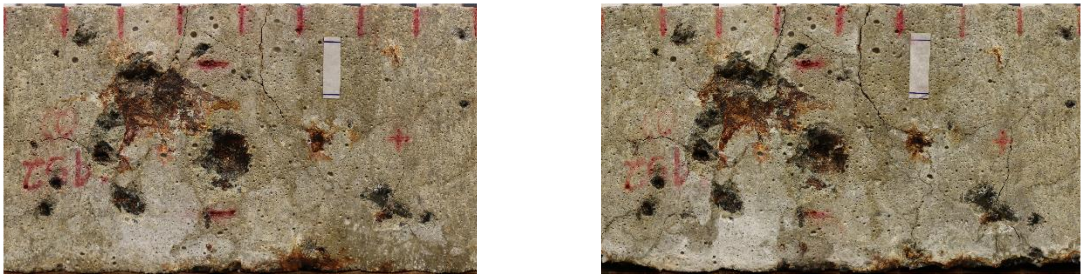

P5 (0.6), body, 42 days P5 (0.6), body, 77 days

P5 (0.4), NaCl face, 42 days P5 (0.4), NaCl face, 140 days

P5 (0.4), body, 42 days P5 (0.4), body, 140 days

Figure 2: Crack evolution of G1 specimens at 42 days and end of exposure.

Effect on Dynamic Elastic Modulus:

Figure 3 shows the relative $E_{dyn,c}$ results for G1 specimens, calculated from the RF testing results presented in Table 4. From the results, C1 (0.6) initially showed a sharp increase in $E_{dyn,c}$ during the first 21 days after testing commenced, after which it remained relatively stable. The initial increase in $E_{dyn,c}$ is mainly attributed to the strength gain from cement hydration, curing and matrix densification. Strength gain was expected, as testing commenced at 14 days, and concrete typically continues to gain strength until about 28 days. The subsequent stability in $E_{dyn,c}$ indicates that the C1 samples did not experience any decrease in strength throughout the testing period. This observation aligns with the visual inspection results, as no signs of oxidation or cracking were observed during the testing period.

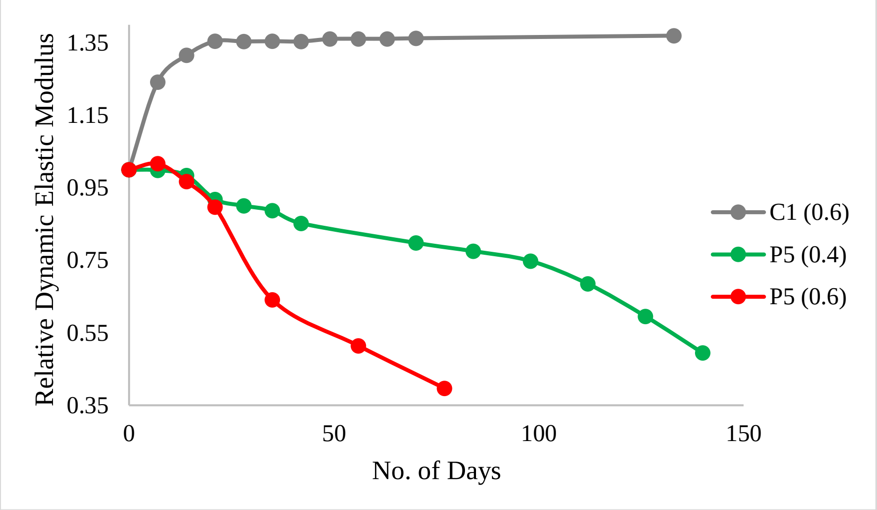

Figure 3: $E_{dyn,c}$ plots for G1 specimens.

On the contrary, the pyrrhotite-containing specimens exhibited a significant decrease in $E_{dyn,c}$ throughout the testing period, except for the first 7 days, during which a slight increase in $E_{dyn,c}$ was observed. Similar to the observed damage and cracking, the drop in $E_{dyn,c}$ was more pronounced in the P5 (0.6) specimens compared to the P5 (0.4) specimens. By 77 days, the P5 (0.6) specimen had experienced a 60% drop in $E_{dyn,c}$, which was 9% more than the 41% drop in P5 (0.4), despite the test duration of P5 (0.6) being almost half that of P5 (0.4). These results further indicate that the w/c ratio plays a role in the deterioration rate of pyrrhotite-containing concrete. Additionally, they suggest that a lower w/c ratio can slow down but not completely prevent deterioration in affected concretes. However, further investigation is still required for even lower w/c ratios.

Table 4: Resonance Frequency and Dynamic Elastic Modulus Results for G1

Number of Days			0	7	14	21	28	35	42	49	56	63	70	77	84	98	112	126	133	140
C1 (0.6)	**(1)**	**RF (Hz)**	6671	7435	7675	7799	7798	7798	7801	7818	7820	7820	7824	-	-	-	-	-	7848	-
		STD	1.00	1.00	0.48	0.48	0.48	0.48	0.48	0.00	0.00	0.00	0.48	-	-	-	-	-	0.48	-
		DEM (GPa)	23.3	29.0	30.9	32.0	31.9	31.9	31.9	32.1	32.1	32.1	32.1	-	-	-	-	-	32.2	-
		Rel. DEM	1.00	1.24	1.33	1.37	1.37	1.37	1.37	1.38	1.38	1.38	1.38	-	-	-	-	-	1.38	-
	(2)	**RF (Hz)**	6745	7508	7694	7779	7781	7781	7782	7804	7805	7806	7820	-	-	-	-	-	7852	-
		STD	0.48	0.00	0.00	0.48	0.48	0.00	0.48	0.48	0.00	0.48	0.48	-	-	-	-	-	0.48	-
		DEM (GPa)	23.3	28.9	30.4	31.2	31.2	31.2	31.2	31.4	31.4	31.4	31.4	-	-	-	-	-	31.6	-
		Rel. DEM	1.00	1.24	1.31	1.34	1.34	1.34	1.34	1.34	1.34	1.34	1.35	-	-	-	-	-	1.36	-
		Avg DEM	23.3	29.0	30.7	31.6	31.6	31.6	31.6	31.7	31.7	31.7	31.8	-	-	-	-	-	31.9	-
		Avg Rel. DEM	1.00	1.24	1.32	1.35	1.35	1.35	1.35	1.36	1.36	1.36	1.36	-	-	-	-	-	1.37	-
P5 (0.6)	**(1)**	**RF (Hz)**	8657	8725	8505	8239	-	6897	-	-	6179	-	-	5565	-	-	-	-	-	-
		STD	0.48	0.48	0.48	0.48	-	0.48	-	-	1.15	-	-	6.56	-	-	-	-	-	-
		DEM (GPa)	31.3	31.9	30.4	28.5	-	20.0	-	-	16.0	-	-	12.9	-	-	-	-	-	-
		Rel. DEM	1.00	1.02	0.97	0.91	-	0.64	-	-	0.41	-	-	0.41	-	-	-	-	-	-
	(2)	**RF (Hz)**	8686	8714	8491	8122	-	6960	-	-	6266	-	-	5406	-	-	-	-	-	-
		STD	0.48	0.00	0.48	0.48	-	0.48	-	-	1.53	-	-	9.64	-	-	-	-	-	-
		DEM (GPa)	28.8	29.2	27.8	25.4	-	18.6	-	-	14.9	-	-	10.9	-	-	-	-	-	-
		Rel. DEM	1.00	1.01	0.96	0.88	-	0.64	-	-	0.42	-	-	0.38	-	-	-	-	-	-
		Avg DEM	30.1	30.6	29.1	27.0	-	19.3	-	-	15.5	-	-	11.9	-	-	-	-	-	-
		Avg Rel. DEM	1.00	1.02	0.97	0.90	-	0.64	-	-	0.41	-	-	0.40	-	-	-	-	-	-
P5 (0.4)	**(1)**	**RF (Hz)**	8104	8036	7992	7685	7582	7491	7334	-	-	-	7040	-	6942	6863	6559	6146	-	5547
		STD	0.48	0.48	0.48	0.00	0.48	0.48	1.15	-	-	-	0.48	-	0.48	0.48	0.48	3.06	-	1.53
		DEM (GPa)	35.9	35.4	35.0	32.5	31.7	31.0	29.7	-	-	-	27.4	-	26.6	26.1	23.8	20.9	-	17.1
		Rel. DEM	1.00	0.99	0.98	0.91	0.88	0.86	0.83	-	-	-	0.76	-	0.74	0.73	0.66	0.48	-	0.48
	(2)	**RF (Hz)**	8094	8127	8032	7772	7712	7680	7527	-	-	-	7326	-	7205	7033	6748	6266	-	5776
		STD	0.48	0.48	0.48	0.48	0.48	0.48	0.48	-	-	-	0.48	-	0.48	0.48	0.48	2.65	-	2.00
		DEM (GPa)	35.2	35.7	34.9	32.8	32.4	32.1	30.9	-	-	-	29.4	-	28.5	27.1	24.9	21.4	-	18.1
		Rel. DEM	1.00	1.01	0.99	0.93	0.92	0.91	0.88	-	-	-	0.83	-	0.81	0.77	0.71	0.61	-	0.41
		Avg DEM	35.6	35.5	35.0	32.6	32.0	31.5	30.3	-	-	-	28.4	-	27.6	26.6	24.4	21.2	-	17.6
		Avg Rel. DEM	1.00	1.00	0.98	0.92	0.90	0.89	0.85	-	-	-	0.80	-	0.78	0.75	0.69	0.60	-	0.49

Effect of Type of Cement – Group 2 (G2):

In G2, the primary objective was to compare the effect of different type of cements on the deterioration rate of pyrrhotite-containing specimens.

Effects on Damage and Cracking:

P5 (OW), NaCl face, 14 days

P5 (OW), NaCl face, 42 days

P5 (OW), body, 14 days

P5 (OW), body, 42 days

C1 (OW), NaCl face, 42 days

C1 (OW), NaCl face, 91 days

C1 (OW), body, 42 days

C1 (OW), body, 91 days

Figure 4 illustrates the evolution of the P5 and C1 specimens cast with Oil-Well Class G High Sulfate Resistant (HSR) cement. For the P5 (OW) sample, cracks were observed on the NaCl-exposed surface of the cylinder. Additionally, reddish-brown stains, indicative of pyrrhotite oxidation, were visible alongside the cracks and popouts. Although the oil-well cement used is known for its high sulfate resistance, visible deterioration occurred as early as the first week (7 days) of the electrochemical accelerated test. The initial cracks on the cylinder body were noted for both P5 (OW) specimens at that time. In contrast, the C1 specimens cast with oil-well cement exhibited only minor discoloration and showed no cracks or popouts throughout the 91 days of testing.

P5 (OW), NaCl face, 14 days

P5 (OW), NaCl face, 42 days

P5 (OW), body, 14 days

P5 (OW), body, 42 days

C1 (OW), NaCl face, 42 days

C1 (OW), NaCl face, 91 days

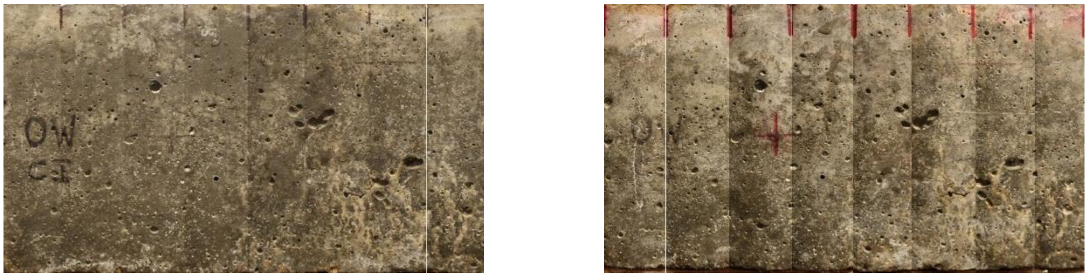

C1 (OW), body, 42 days

C1 (OW), body, 91 days

Figure 4 Crack evolution of G2 specimens for Oil-Well cement at early stages and end of exposure.

Figure 5 presents photographs of the P5 and C1 specimens cast with White I cement. In the P5 (W) sample, which contains pyrrhotite, oxidation stains and cracks became apparent after 7 days of testing, with significant worsening observed progressively throughout the testing period, culminating at 77 days in the electrochemical accelerated test. Cracks were seen throughout the cylinder body, including the NaCl-exposed surface. In contrast, the control specimens C1 (W) showed no visible signs of deterioration, with no cracks or popouts observed during the 77-day testing period.


P5 (W), NaCl face, 14 days

P5 (W), NaCl face, 77 days

P5 (W), body, 14 days

P5 (OW), body, 77 days


C1 (W), NaCl face, 14 days

C1 (W), NaCl face, 77 days

C1 (W), body, 14 days

C1 (W), body, 77 days

Figure 5 Crack evolution of G2 specimens for White cement at early stages and end of exposure.

Effect on Dynamic Elastic Modulus:

Figure 6 shows that for the C1 samples of both cement types, the dynamic elastic modulus exhibited a more pronounced increase during the first 30 days of testing. This increase is likely due to strength gain from curing and matrix densification. A slight increase in modulus was observed until day 40, followed by stabilization of the values.

The same figure presents the results for the P5 samples cast with both Oil-Well Class G High Sulfate Resistant (HSR) cement and White I cement. For the P5 (OW) samples, the dynamic elastic modulus decreased from day one, with a more pronounced drop after 20 days, continuing until the test was terminated. In contrast, the P5 (W) samples also showed a decrease, although this decline was less sharp and less pronounced compared to the P5 (OW) samples. The decrease in modulus became more significant after 50 days and remained relatively stable between days 60 and 80.

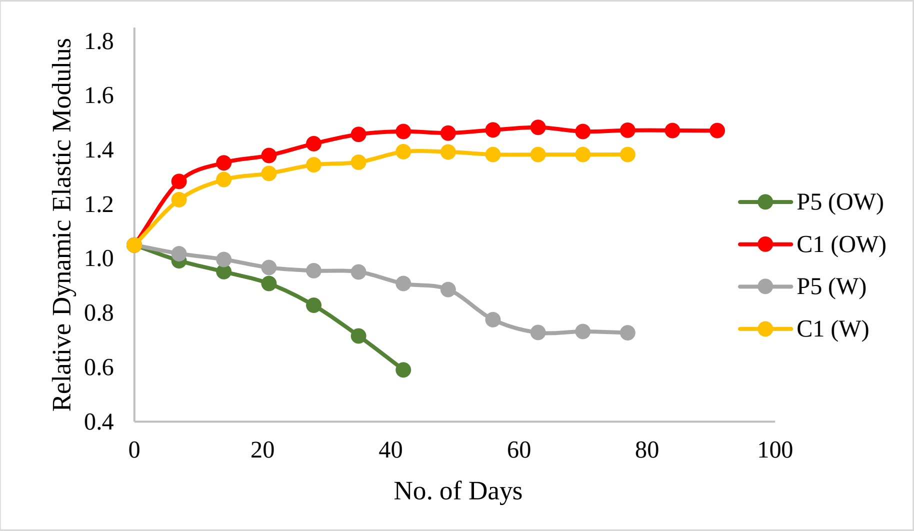

Figure 6 $E_{dyn,c}$ plots for G2 specimens

Table 5 Resonance Frequency and Dynamic Elastic Modulus Results for G2

Number of Days			0	7	14	21	28	35	42	49	56	63	70	77	84	91
P5 (OW)	**1**	**RF (Hz)**	9504	9353	9117	8907	8871	7994	7866	-	-	-	-	-	-	-
		STD	2.89	3.06	2.08	2.65	6.03	10.44	2.31	-	-	-	-	-	-	-
		DEM (GPa)	41.8	40.4	38.4	36.7	36.3	29.4	28.5	-	-	-	-	-	-	-
		Rel. DEM	1.00	0.97	0.92	0.88	0.87	0.70	0.68	-	-	-	-	-	-	-
	2	**RF (Hz)**	9756	9339	9169	8936	8091	7737	6197	-	-	-	-	-	-	-
		STD	2.00	5.51	15.53	5.03	2.08	3.43	7.21	-	-	-	-	-	-	-
		DEM (GPa)	43.7	40.0	38.6	36.6	30.0	27.4	17.5	-	-	-	-	-	-	-
		Rel. DEM	1.00	0.92	0.88	0.84	0.69	0.63	0.40	-	-	-	-	-	-	-
		Avg DEM	42.7	40.2	38.5	36.6	33.2	28.4	23.0	-	-	-	-	-	-	-
		Avg Rel. DEM	1.0	0.9	0.9	0.9	0.8	0.7	0.4	-	-	-	-	-	-	-
C1 (OW)	**1**	**RF (Hz)**	6945	7727	7892	7956	8125	8306	8342	8262	8283	8321	8278	8248	8229	8216
		STD	2.65	3.06	3.00	3.61	2.08	1.73	2.08	4.16	1.53	1.16	8.19	3.51	2.08	4.04
		DEM (GPa)	25.0	31.1	32.4	32.9	34.2	35.8	36.0	35.3	35.4	35.7	35.3	35.0	34.8	34.6
		Rel. DEM	1.00	1.24	1.30	1.32	1.37	1.43	1.44	1.41	1.42	1.43	1.41	1.40	1.40	1.39
	2	**RF (Hz)**	6779	7505	7764	7860	7955	7977	8019	8065	8113	8132	8094	8152	8170	8189
		STD	0.48	2.65	5.03	16.07	2.65	4.73	2.08	4.93	2.89	4.73	2.52	6.24	4.51	1.73
		DEM (GPa)	24.2	29.7	31.7	32.5	33.3	33.5	33.8	34.2	34.6	34.7	34.4	34.9	35.1	35.2
		Rel. DEM	1.00	1.22	1.31	1.34	1.38	1.38	1.40	1.41	1.43	1.43	1.42	1.44	1.45	1.45
		Avg DEM	24.6	30.4	32.0	32.7	33.8	34.6	34.9	34.7	35.0	35.2	34.9	35.0	35.0	34.9
		Avg Rel. DEM	1.00	1.23	1.30	1.33	1.37	1.41	1.42	1.41	1.42	1.43	1.42	1.42	1.42	1.42
P5 (W)	**1**	**RF (Hz)**	7820	7726	7696	7614	7581	7569	7553	7494	7481	7082	6467	6447	-	-
		STD	4.36	11.55	4.73	2.65	0.48	4.36	10.69	6.43	5.57	4.04	1.00	5.29	-	-
		DEM (GPa)	33.4	32.6	32.4	31.7	31.4	31.3	31.1	30.6	30.4	27.3	22.8	22.6	-	-
		Rel. DEM	1.00	0.98	0.97	0.95	0.94	0.94	0.93	0.92	0.91	0.82	0.68	0.68	-	-
	2	**RF (Hz)**	7913	7756	7614	7454	7391	7372	7014	6887	5810	5809	-	-	-	-
		STD	8.33	3.06	3.51	1.15	9.54	2.65	6.51	2.89	3.79	9.00	-	-	-	-
		DEM (GPa)	34.6	33.2	32.0	30.7	30.2	30.0	27.1	26.2	18.6	18.6	-	-	-	-
		Rel. DEM	1.00	0.96	0.93	0.89	0.87	0.87	0.78	0.76	0.44	0.44	-	-	-	-
		Avg DEM	34.0	32.9	32.2	31.2	30.8	30.6	29.1	28.4	24.6	23.0	22.8	22.6	-	-
		Avg Rel. DEM	1.00	0.97	0.95	0.92	0.91	0.90	0.86	0.84	0.73	0.68	0.68	0.68	-	-
C1 (W)	**1**	**RF (Hz)**	7406	8041	8301	8442	8491	8543	8723	8725	8664	8661	8657	8657	-	-
		STD	2.65	3.21	1.15	1.00	5.51	6.08	2.65	14.36	2.52	4.00	2.08	2.52	-	-
		DEM (GPa)	28.0	33.0	35.1	35.6	36.7	37.2	38.7	38.8	38.2	38.2	38.1	38.1	-	-
		Rel. DEM	1.00	1.18	1.26	1.27	1.31	1.33	1.38	1.39	1.37	1.36	1.36	1.36	-	-
	2	**RF (Hz)**	7393	7947	8184	8281	8362	8380	8446	8448	8450	8455	8461	8464	-	-
		STD	1.00	1.53	1.53	1.00	5.51	2.52	14.36	4.04	3.79	3.61	2.08	1.73	-	-
		DEM (GPa)	28.9	33.4	35.4	36.2	36.9	37.0	37.6	37.6	37.6	37.6	37.6	37.7	-	-
		Rel. DEM	1.00	1.16	1.23	1.25	1.28	1.28	1.30	1.30	1.30	1.30	1.30	1.30	-	-
		Avg DEM	28.4	33.2	35.3	35.9	36.8	37.1	38.2	38.2	37.9	37.9	37.9	37.9	-	-
		Avg Rel.DEM	1.00	1.17	1.24	1.26	1.29	1.30	1.34	1.34	1.33	1.33	1.33	1.33	-	-

Conclusion:

This study initiated the investigation of the effectiveness of concrete mix design mitigation methods on the evolution of deterioration of cement concrete containing pyrrhotite reactive minerals. The electrochemical acceleration testing (EAT) and damage evaluation methods were successfully set up, implemented, and applied. The following two concrete mix design parameters were selected in this preliminary study: water to cement (w/c) ratio and type of cement.

The summary of key findings from the study based on the obtained results are presented below:

- Control specimens without pyrrhotite exhibited no visible signs of damage and stable dynamic elastic modulus values throughout the testing period.
- Pyrrhotite-containing specimens showed visible signs of deterioration such as discoloration, concrete pop-outs and cracking, and significant decreases in dynamic elastic modulus as testing progressed.
- Specimens with a lower w/c ratio (0.4) demonstrated slower deterioration rates and higher resistance with higher modulus of elasticity than those with a higher w/c ratio (0.6).
- Lower w/c ratios can slow down deterioration by densifying the matrix, which increases the resistance to deterioration and cracking from localized stresses.
- Specimens with cement containing lower C_4AF, although presented damage, presented less pronounced decrease in dynamic elastic modulus when compared to cement specimens with lower C_3A.
- Specimens with cement containing lower C_3A presented deterioration and pronounced decrease in dynamic elastic modulus.

While a lower w/c ratio improves resistance to damage, it does not prevent degradation in pyrrhotite-containing concrete specimens. Further reduction in w/c ratios may be necessary to enhance durability. Meanwhile, although the specimens with low C_4AF content showed greater resistance in the electrochemical accelerated test compared to those with low C_3A content, deterioration was still observed. Further testing and detailed microstructural analysis are required to identify the specific phases formed in each specimen and to better understand the mechanisms driving degradation.

Reference List

[1] M. Ojo, D. Kim, L. Frame, K. Wille, Electrochemical investigation of accelerated deterioration of concrete with iron-sulfide containing aggregates, Cement and Concrete Research. 182 (2024).

[2] R. Castillo Araiza, A. Rodrigues, B. Fournier, J. Duchesne, A new accelerated testing scheme to evaluate the potential oxidation reaction of sulfide-bearing aggregates in concrete specimens, Cement and concrete research. 180 (2024) 107507.

[3] R. Castillo Araiza, B. Fournier, J. Duchesne, A. Rodrigues, Electrochemical activation of oxidation of sulfide-bearing aggregates in concrete specimens, Cem. Concr. Res. 170 (2023) 107186.

[4] NT BUILD 492, Concrete, Mortar and Cement-Based Repair Materials: Chloride Migration Coefficient from Non-Steady-State Migration Experiments, Nordtest Method. (1999).

[5] C09 Committee, ASTM C1202-22, Test Method for Electrical Indication of Concretes Ability to Resist Chloride Ion Penetration, ASTM International. (2022).

[6] R. Zhong, K. Wille, Deterioration of residential concrete foundations: The role of pyrrhotite-bearing aggregate, Cement & concrete composites. 94 (2018) 53–61.

[7] X. Jiang, S. Mu, Z. Yang, J. Tang, T. Li, Effect of temperature on durability of cement-based material to physical sulfate attack, Construction and Building Materials. 266 (2021).

[8] T. Hirsch, T. Matschei, D. Stephan, The hydration of tricalcium aluminate (Ca3Al2O6) in Portland cement-related systems: A review, 168 (2023) 107150.

[9] A. Hossack, M. Thomas, Evaluation of the effect of tricalcium aluminate content on the severity of sulfate attack in Portland cement and Portland limestone cement mortars, Cement and Concrete Composites. 56 (2015) 115–120.

[10] P. Barnes, J. Bensted, Structure and Performance of Cements, CRC Press, 2001.

[11] S. Ye, P. Feng, Y. Liu, J. Liu, J. Bullard, Dissolution and early hydration of tricalcium aluminate in aqueous sulfate solutions, Cem. Concr. Res. 137 (2020) 106191.

[12] C09 Committee, ASTM C192/C192M-19, Practice for Making and Curing Concrete Test Specimens in the Laboratory, ASTM International. 10 (2020).

[13] C09 Committee, ASTM C215-19, Test Method for Fundamental Transverse, Longitudinal, and Torsional Resonant Frequencies of Concrete Specimens, ASTM International. (2020).

Task 3: Developing the Scope of Work

Prepared by: Kay Wille

Study Objectives

Future testing and research tasks were developed. This required close collaboration between the PI, co-PIs, research personnel and the MassDOT project champion and technical representative. Updates were provided and discussed during regular virtual meetings with the project champion and technical representative.

Developing the Scope of Work

In close collaboration between the PI, co-PIs, research personnel and the MassDOT project champion and technical representative, future testing and research tasks were discussed during regular virtual meetings and are summarized below.

- Investigate the deterioration behavior of various concrete mixture designs including reference and pyrrhotite bearing aggregates. These mixtures include variation in the w/c ratio, the use of supplemental cementitious materials, such as fly ash or ground granulated blast furnace slag. In particular, the various mixtures designs also include the MassDOT high-performance (HP) concrete mixture.
- Investigation of other potential mitigation methods on the deterioration rate of affected concrete mixtures. This potentially include colloidal silica sealers, sodium-silicates, water-proofing / hydrophobic admixture, and corrosion inhibitor admixtures.
- Collaboration with companies and their products might be beneficial and necessary.

Further detailed information is included in a follow-up proposal, which is currently in development.